Supporting Information

Light Assisted Coupling of Phenols with CO_2 to 2-Hydroxy-benzaldehydes Catalyzed by g-C_3N_4 /NH_2-MIL-101(Fe) composite

Sakshi Bhatt,[1,2] Ranjita S. Das[3], Anupama Kumar[3], Anil Malik,[1,2] Aishwarya Soni[1], Suman L Jain,[1*]

[1]*Chemical & Material Sciences Division, CSIR-Indian Institute of Petroleum, Haridwar Road, Mohkampur, Dehradun-248005, India.*

[2]*Academy of Scientific and Innovative Research,* Ghaziabad- 201002, India.

[3]*Visvesvaraya National Institute of Technology (VNIT) Nagpur-440010 India*

[*]Corresponding Author: suman@iip.res.in, +911352525788

Content:

Characterization Techniques

UV-VIS absorption spectra of the samples were recorded on Perkin Elmer Lambda 750 UV-VIS-NIR spectrophotometer with a 10-mm quartz cell using $BaSO_4$ as a reference. High-resolution transmission electron microscopy (HR-TEM) was done using a JEM 2100 (JEOL, Japan) microscope by mounting the ethanol dispersed sample on a Lacey carbon-coated Cu grid. A field emission scanning electron microscope (FESEM) (JEOL JSM7610F) equipped with an EDS (Oxford Instruments) was used for the determination of the morphological features of the samples. X-ray diffraction (XRD) pattern was recorded to determine the crystallinity of the materials using Bruker D8 Advance diffractometer at 40 kV and 40 mA with Cu Kα radiation (λ= 0.15418 nm). The scan range was 2θ = 20 ^oC to 70 ^oC with a scan rate of 0.02 °C/s. The BET surface area (S_{BET}), pore volume (VP), and mean pore diameter (RP) of composites were estimated using N_2 adsorption-desorption isotherm at 77K using BELSORP-max TPD pro-Chem Master analyzer. All the samples were degassed at 200 ^oC for 3h under N_2 atmosphere. Fourier transform infrared spectroscopy (FT-IR) was used to determine the stretching and bending vibrations and was recorded in the range of 4000–400 cm^{-1} on an AlphaBruker FTIR spectrometer with a wavenumber resolution of 4 cm^{-1} in the transmission mode in spectroscopic grade KBr pellets for all the powders. X-ray photoelectron spectroscopy (XPS) analysis was performed on KRATOS AXIS 165 with Mg Kα irradiation. Thermogravimetric analysis (TGA) was carried out using a thermal analyzer TASDT Q-600. The thermogravimetric analysis determined the thermal degradation pattern of the materials in the temperature range of 40-800 ^oC under nitrogen flow with a scan rate of 10 ^oC/min heating rate. The photoelectrochemical analysis (PEC), such as cyclic voltammetry (CV), linear sweep voltammetry (LSV), electron impedance spectroscopy (EIS) and mott-schotkey (MS) were performed on Versatat-4 potentiostat in CO_2 saturated 0.1M aqueous $KHCO_3$ solution with Pt as a counter and Ag/AgCl as a reference electrode. The synthesized

material coated on the FTO plate was used as a working electrode. During the analysis, the active surface area of the working electrode was taken as 1 cm^2.

Surface area

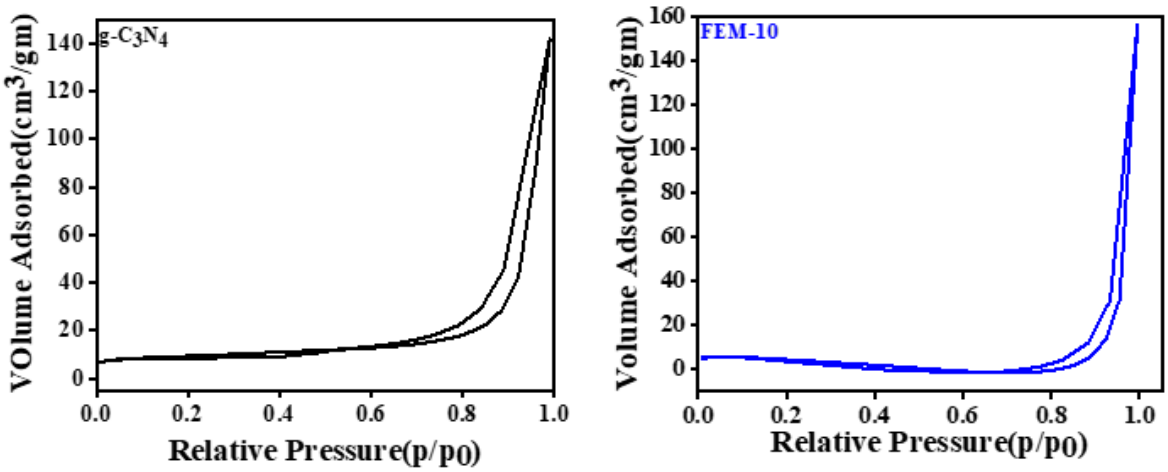

***Figure S1*:** N_2 adsorption-desorption isotherm of g-C_3N_4 and FEM-10

Thermal stability of the samples

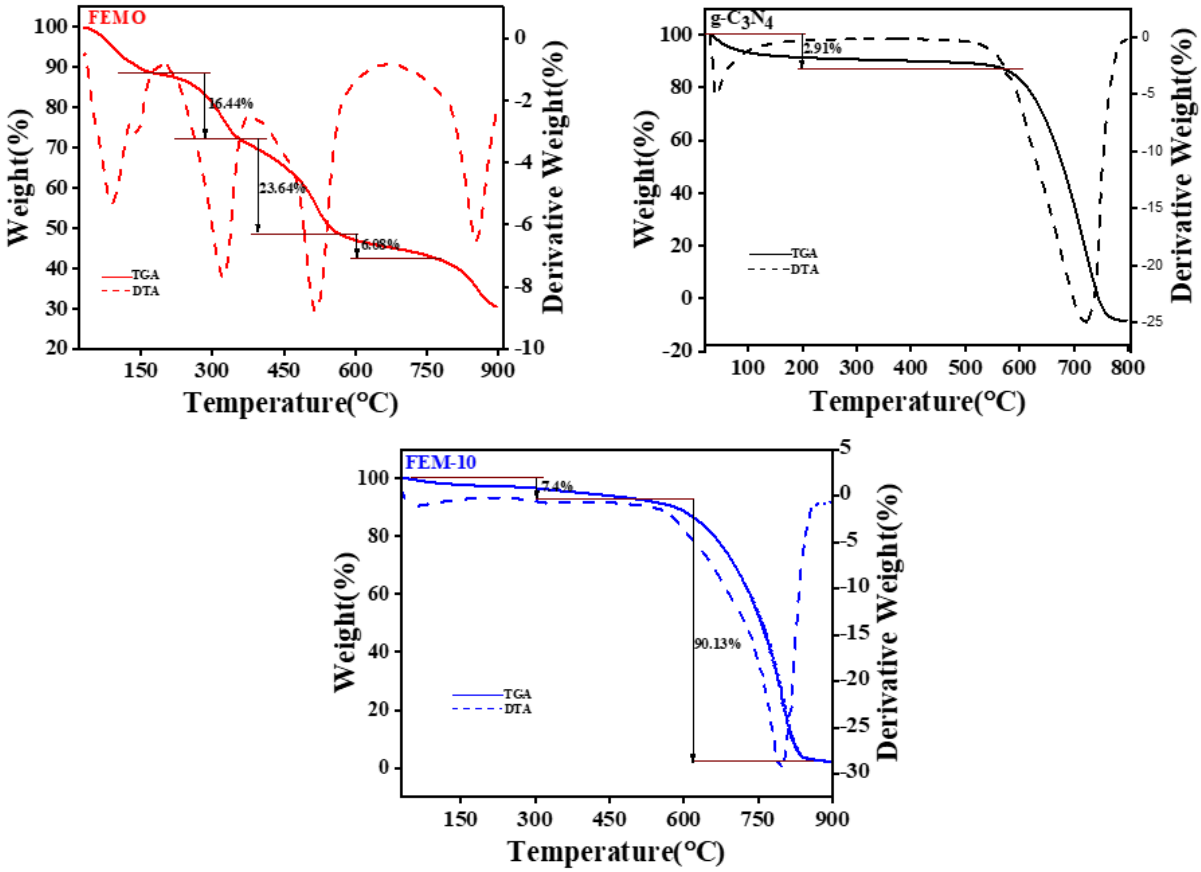

***Figure S2*:** TG/DTA of FEMO, g-C_3N_4 and active photocatalyst FEM-10

Elemental mapping of FEM-10

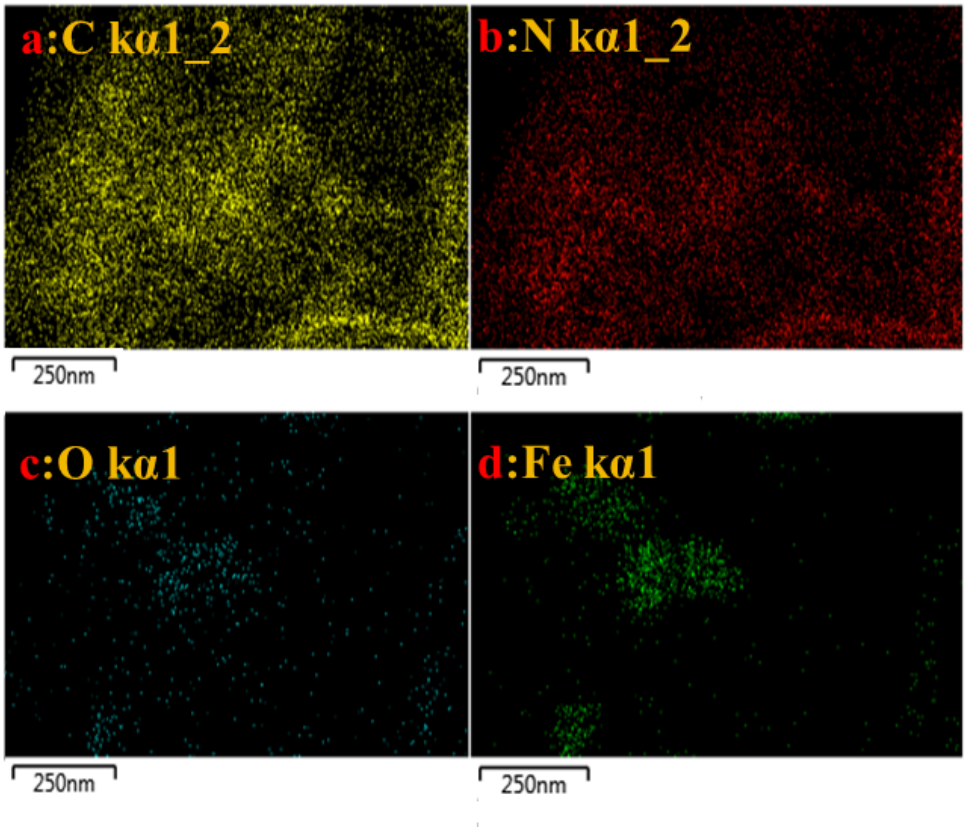

***Figure S3*:** Elemental mapping of (a)-C, (b)-N, (c)-O, and (d)-Fe of FEM-10

FE-SEM of the materials

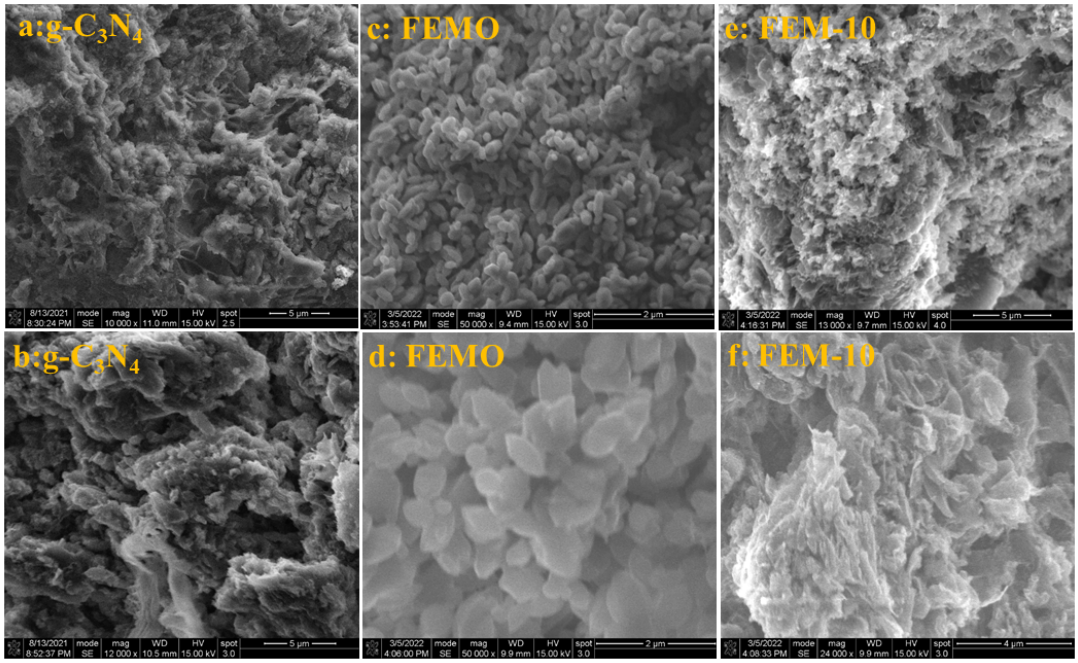

***Figure S4*:** FE-SEM image of (a), (b)-g-C_3N_4, (c), (d)-FEMO and (e), (f)- FEM-10

XPS of FEMO and g-C_3N_4

The elemental composition and electronic state of FEMO were determined using the XPS as presented in *Figure S5*. In the XPS Fe(2p) spectra of FEMO, two peaks at binding energy 711.8 eV and 725.5 eV corresponded to Fe($2p_{3/2}$) and Fe($2p_{1/2}$) energy levels, respectively are observed. A single satellite signal is also obtained nearly at 716.0 eV. The deconvoluted O (1s) spectra exhibit two peaks at binding energy 530.9 eV and 532.7 eV, corresponded to the Fe-O and C-O bonds, respectively. The N(1s) XPS spectra reveal two peaks, in which the first peak appeared at 398.5eV is attributed to the H-N-H bond. Another peak at 400.84 eV is related to the protonated amine (NH^+) group. The C(1s) spectra display three peaks at binding energy 284.3eV, 285.3eV and 288.2eV, which are ascribed to the C-C, C-O-C, and C=O bonds.

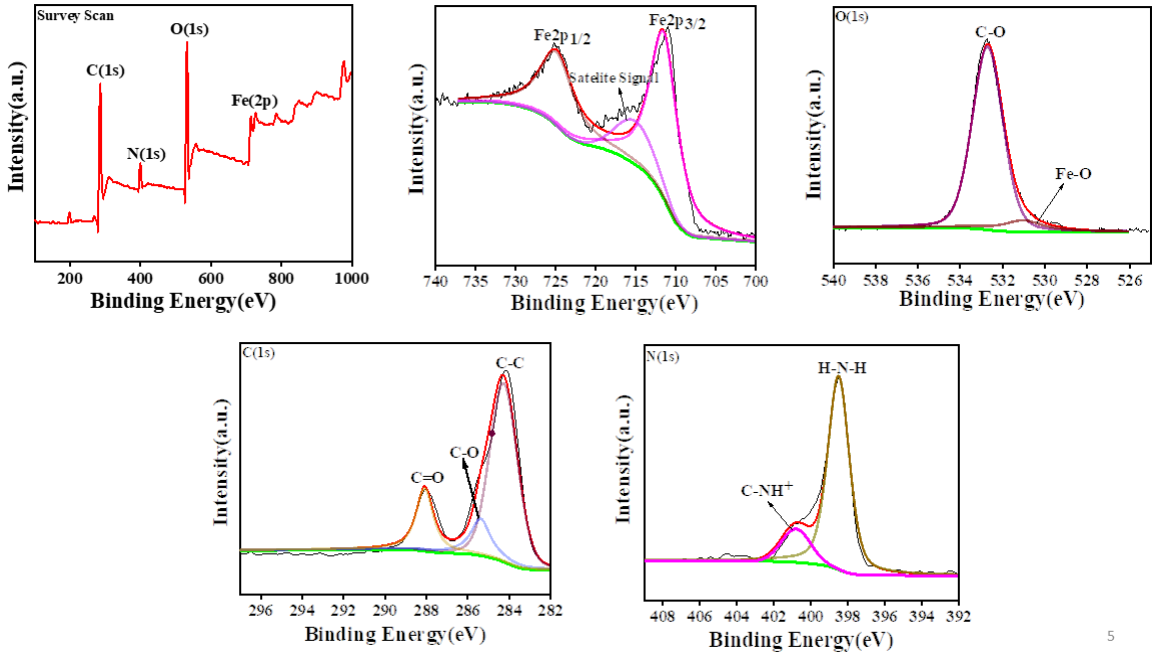

***Figure S5*:** XPS spectra of FEMO

The XPS spectra of prinstine g-C_3N_4 are shown in *Figure S6*. In the XPS spectra of N(1s), three peaks at binding energies 405.4 eV (N-H), 401.2 eV (N=C), and 399.3 eV (C-N) are

appeared. Further, XPS spectra of the C (1s), exhibit three peaks at binding energies 294 eV (C-H), 288.8 eV (N=C), and 285.1 eV (C-C) of g-C_3N_4.

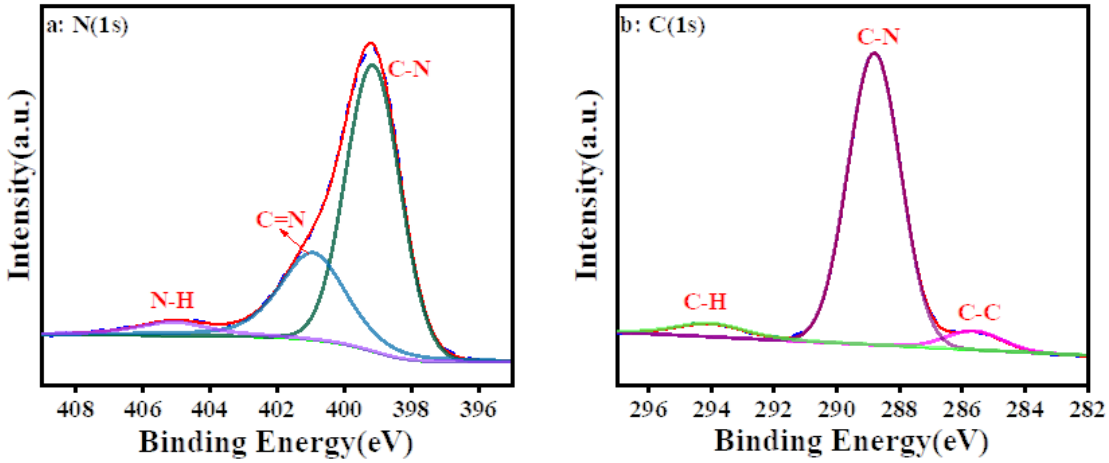

***Figure S6*:** XPS spectra of g-C_3N_4, a) N(1s) and b) O (1s)

Optimized geometry of the reactants, product and involved transition state

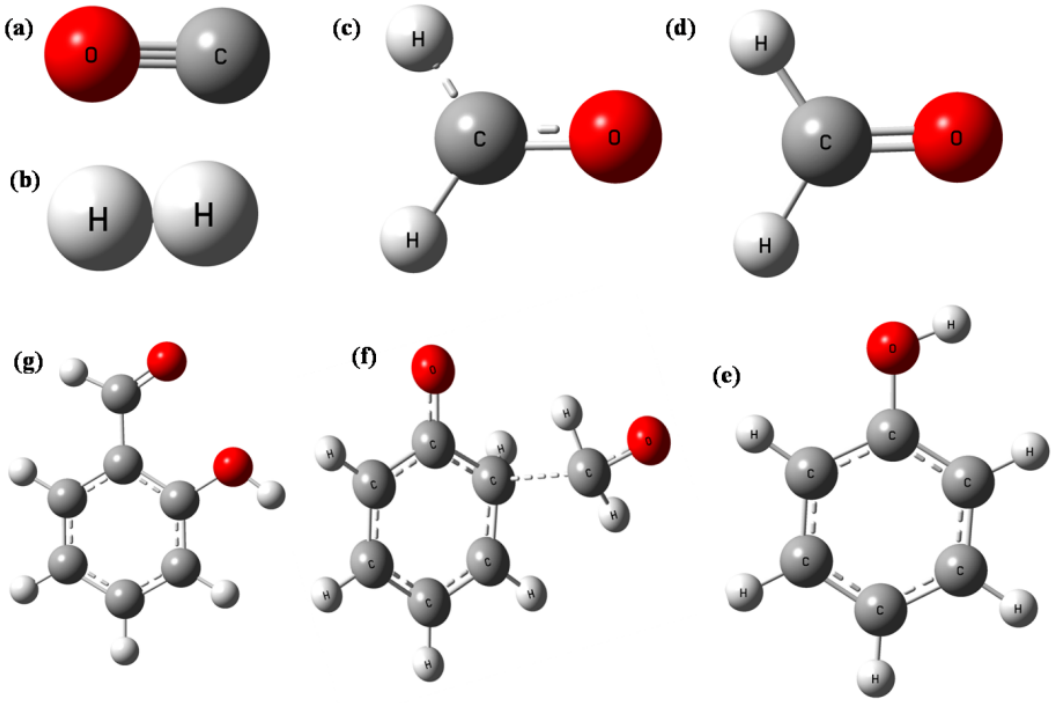

***Figure S7*: optimized geometry of: a) Carbon monoxide, b) H_2 molecule, c) formaldehyde transition state, d) formaldehyde e) phenol, f) transition state between phenol and formaldehyde and g) 2-hydroxyl benzaldehyde.**

Table S1: Physicochemical parameter calculated from molecular simulated calculation

Compounds	**Energy (Hartree)**	**Polarizability (a.u)**	**Dipole moment (Debye)**	**Molecular weight (AMU)**
FEMO complex	-0.81147158	425.68867	19.058014	755.83415
g-C_3N_4-complex	0.19324009	216.30433	0.4432	302.17159
FEMO@ g-C_3N_4 (1:1 ratio) complex	-0.74019602	637.18933	18.017648	1058.0057
FEMO@ g-C_3N_4 (1:2 ratio) complex	-0.52393955	846.91086	34.470675	1360.1773
Carbon dioxide (GO)	-0.021801762	9.3823333	0.1725	27.994915
Hydrogen molecule (H_2)	-0.041006648	1.395	0	2.0156501
Formaldehyde (H_2CO)	-0.032922707	9.8363333	2.8172	30.010565
Phenol (C_6H_5OH)	-0.033276298	51.629	1.3598612	94.041865
o-hydroxyl benzaldehyde (product)	-0.086517929	67.376667	3.3270445	122.03678

Detailed steps of the reaction mechanism for the conversion of phenol to 2-hydroxyl benzaldehyde

Based on the molecular simulation result, the possible reaction mechanism for transformation of phenol to o-hydroxyl benzaldehyde in presence of CO_2 under visible light irradiation was established and described in four different steps as follows-

Step-1

Excitation of electron

According to the simulation study, synthesized FEM-10 catalyst generate electron-hole ($e^- - h^+$) pair in conduction band (CB) and valence band (VB) respectively under visible light irradiation. The generated electron in CB was further used for conversion of CO_2 to CO and H_2 molecule.

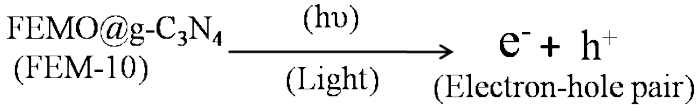

Step-2

Generation of CO and H_2

The generated electron in step-1 was used for photoreduction of Fe atom present in FEM-10 catalyst from Fe^{+3} to Fe^{+2} followed by addition of CO_2 to form FEM-10-CO_2 complex respectively. Afterward, obtained FEM-10-CO_2 complex was passed through various steps like metal ligand charge transfer (MLCT) pathway followed by protonation and dehydration then finally release CO and H_2 molecule. The explained mechanism below was established based on the article reported by J. Lin et al since 2018 with some modification[8]

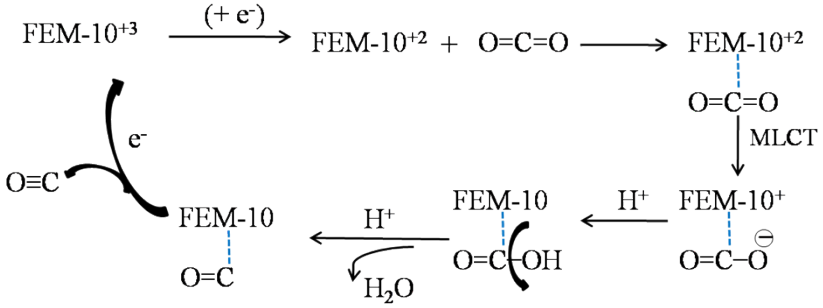

Step-3

Formation of Formaldehyde (reactive species)

In step-3, formaldehyde was generated by the reaction of CO and H_2 release from step-2 via simple nucleophilic addition reaction pathway.

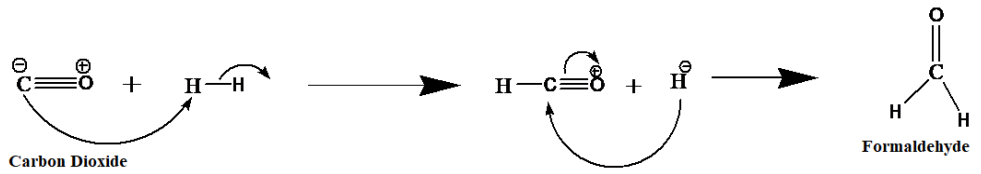

Step-4

Conversion of phenol to o-hydroxyl benzaldehyde

Step-4 described the coupling of phenol with formaldehyde in presence of strong base to form o-hydroxy benzaldehyde. The formaldehyde was attacked to the ortho position of phenol due to its more electron density in ortho and para position as it is an electron donating group. The possible reaction mechanism is given below.

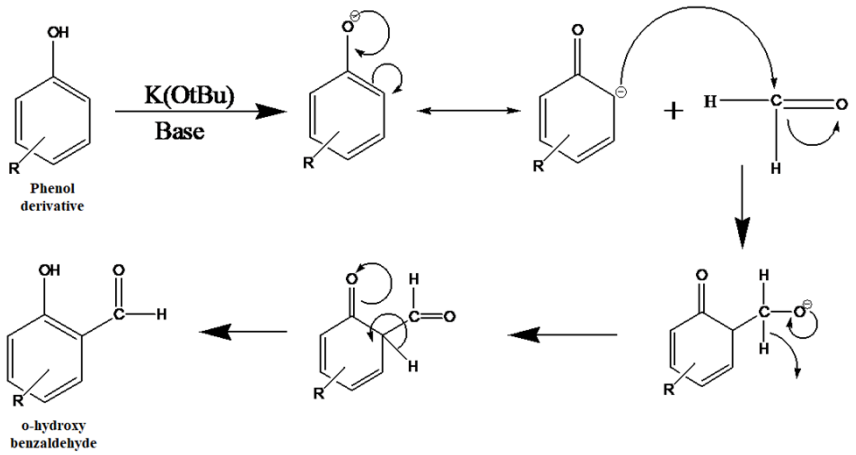

Product characterization data (^{1}H & ^{13}C NMR)

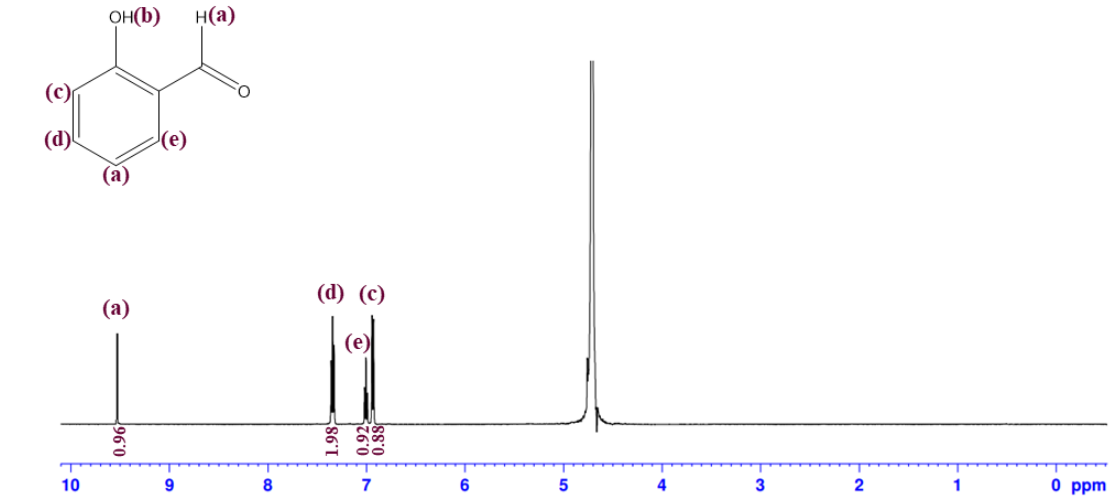

Fig. S8: ^{1}H NMR spectrum of salicylaldehyde(Table-3, entry 1)

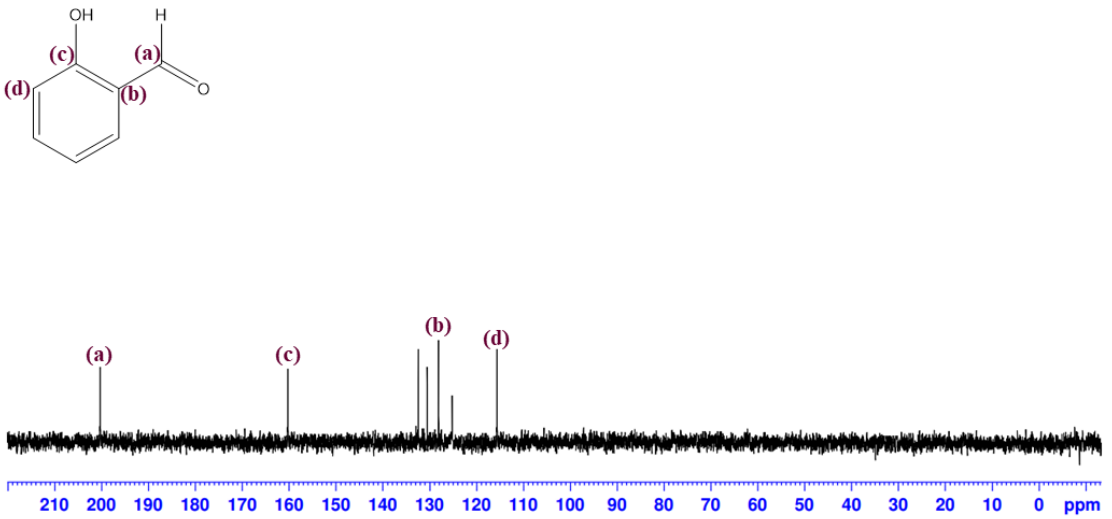

Fig. S9: ^{13}C NMR spectrum of Salicylaldehyde(Table-3, entry 1)

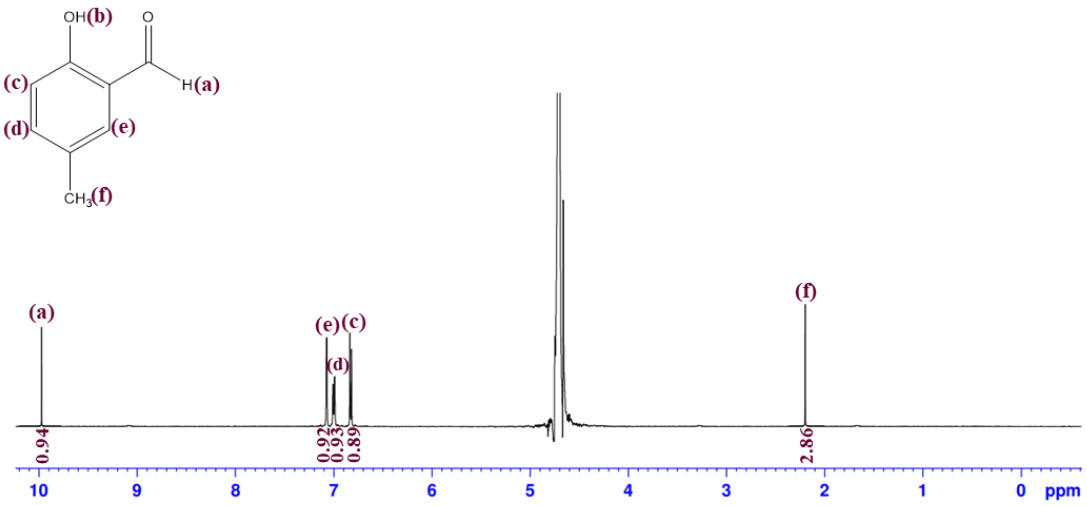

Fig. S10: ^{1}H NMR spectrum of 2-hydroxy-5-methylbenzaldehyde(Table-3, entry 2)

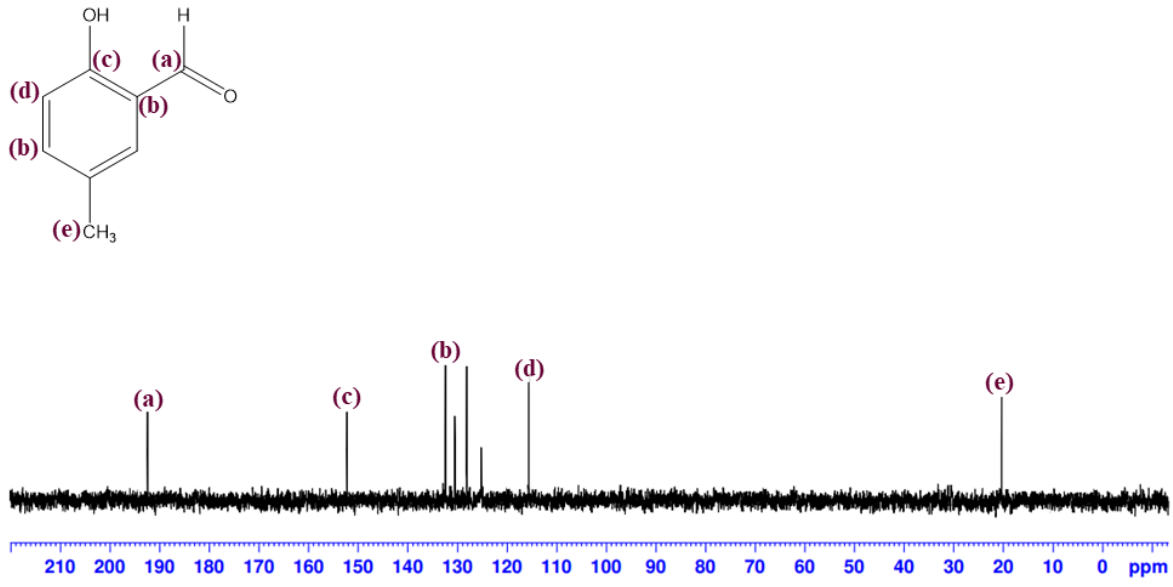

Fig. S11: ^{13}C NMR spectrum of 2-hydroxy-5-methylbenzaldehyde (Table-3, entry 2)

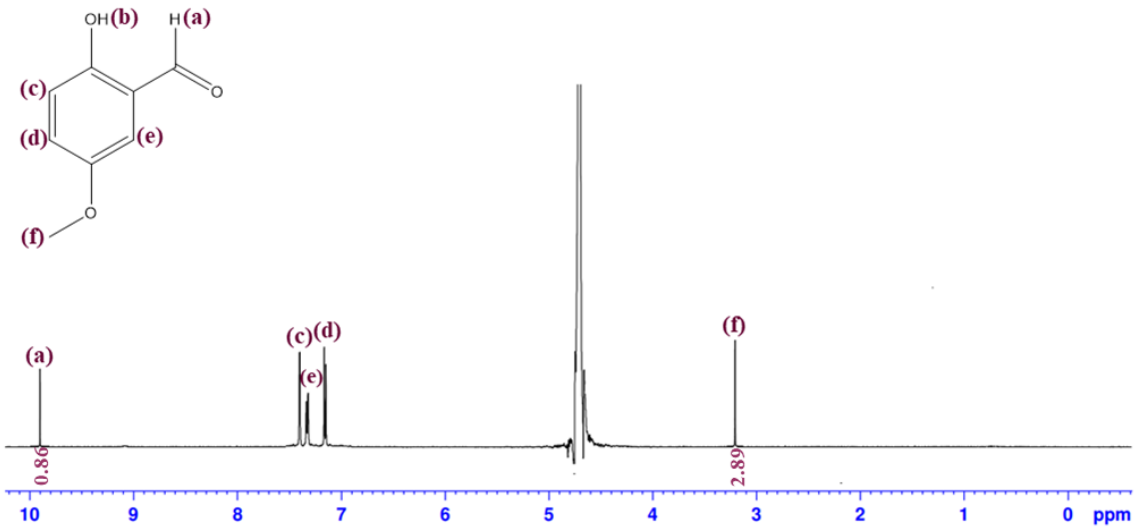

Fig. S12: ^{1}H NMR spectrum of 2-hydroxy-5-methoxybenzaldehyde

(Table-3, entry 3)

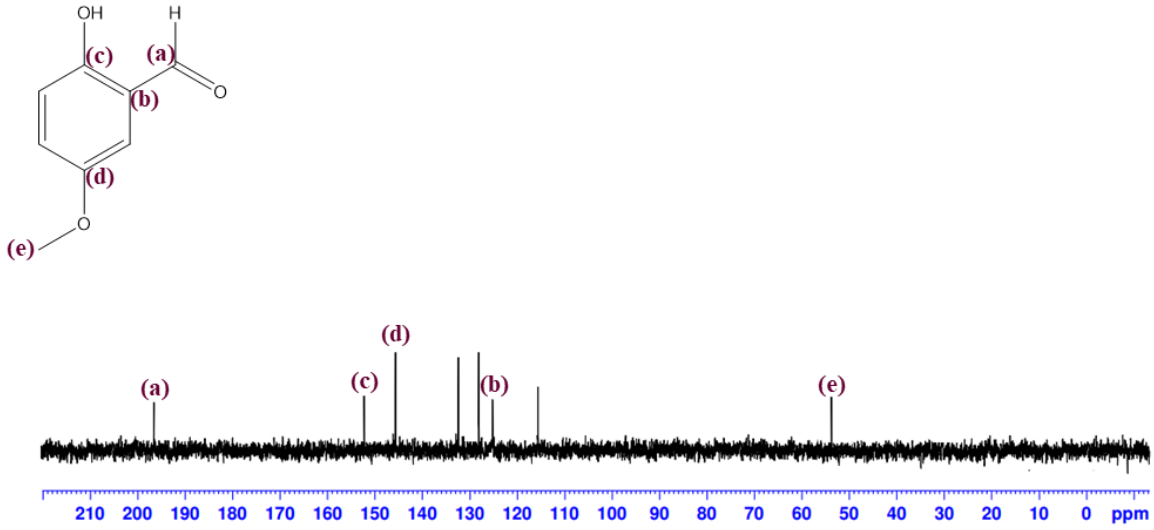

Fig. S13: ^{13}C NMR spectrum of 2-hydroxy-5-methoxybenzaldehyde

(Table-3, entry 3)

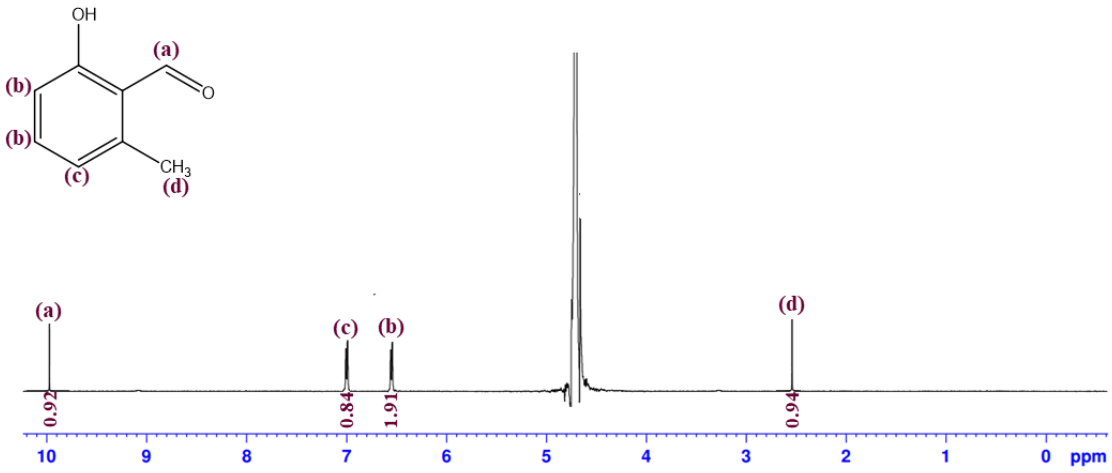

Fig. S14: ^{1}H NMR spectrum of 2-hydroxy-6-methylbenzaldehyde (Table-3, entry 4)

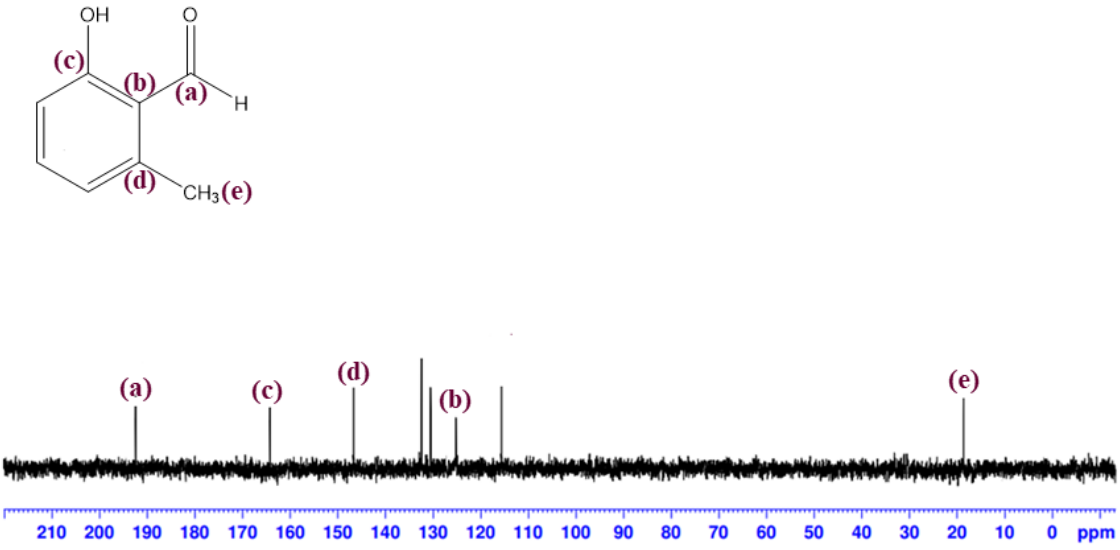

Fig. S15: ^{13}C NMR spectrum of 2-hydroxy-6-methylbenzaldehyde (Table-3, entry 4)

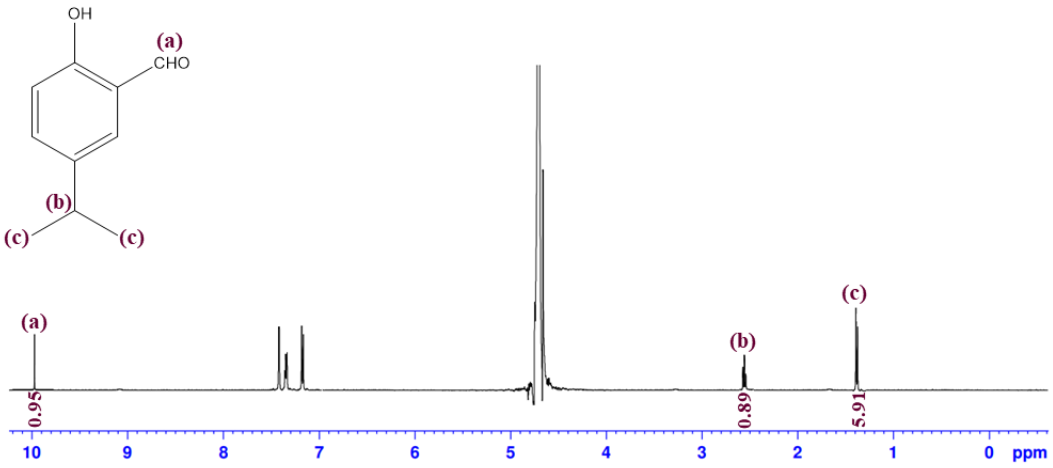

Fig. S16: ^{1}H NMR spectrum of 2-hydroxy-5-isopropylbenzaldehyde (Table-3, entry 5)

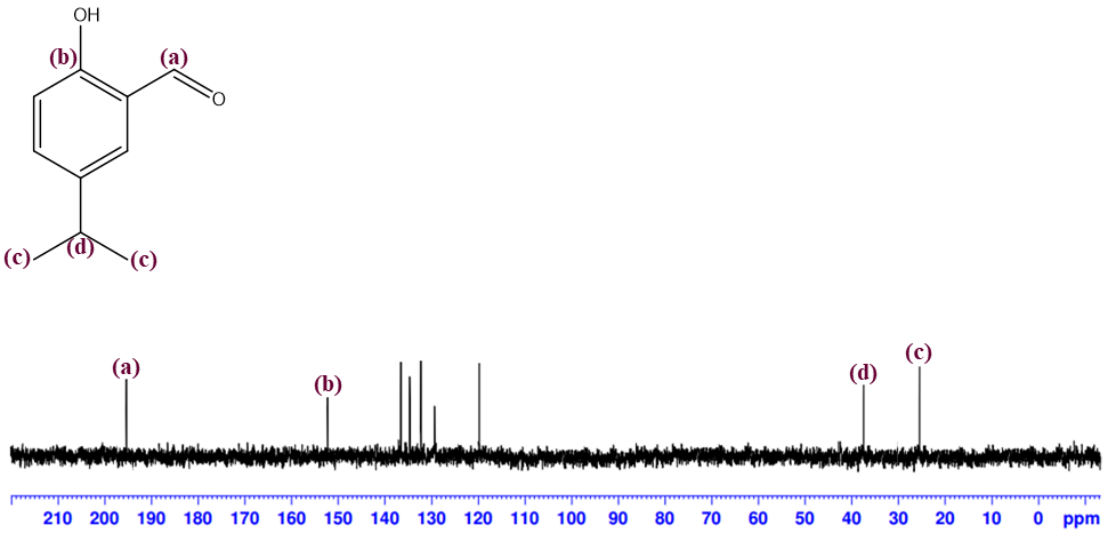

Fig. S17: ^{13}C NMR spectrum of 2-hydroxy-5-isopropylbenzaldehyde (Table-3, entry 5)

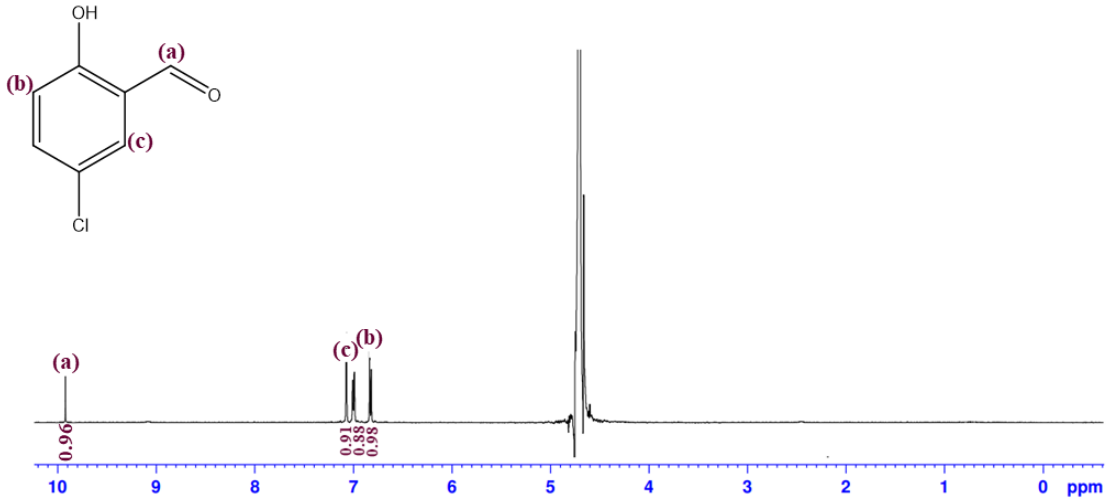

Fig. S18: ^{1}H NMR spectrum of 5-chloro-2-hydroxybenzaldehyde (Table-3, entry 9)

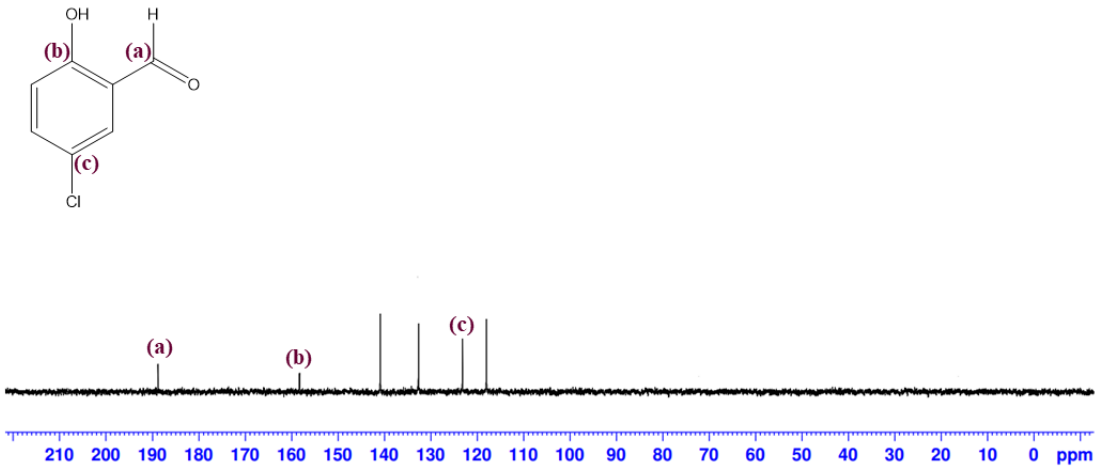

Fig. S19: ^{13}CNMR spectrum of 5-chloro-2-hydroxybenzaldehyde (Table-3, entry 9)

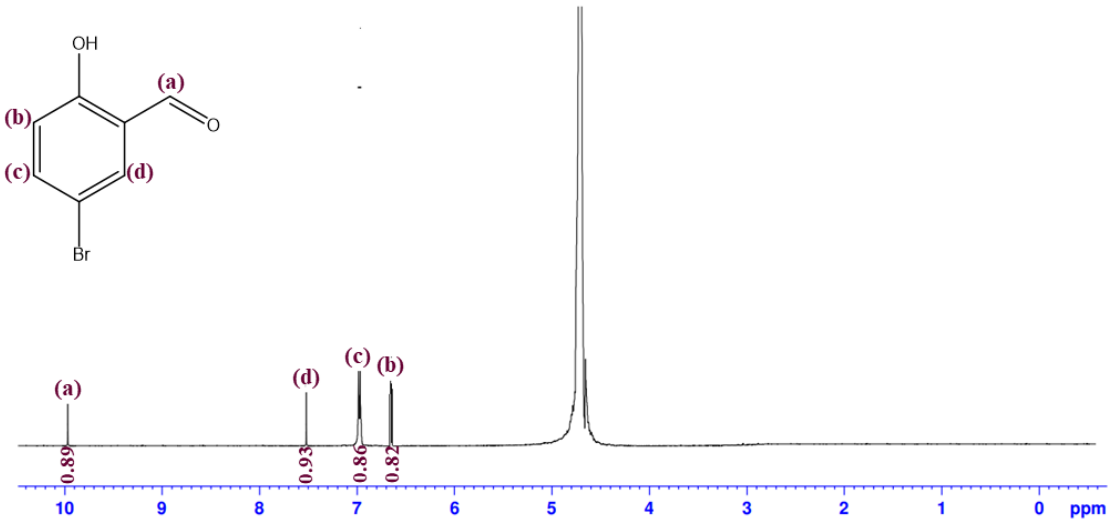

Fig. S20: [1]HNMR spectrum of 5-bromo-2-hydroxybenzaldehyde (Table-3, entry 10)

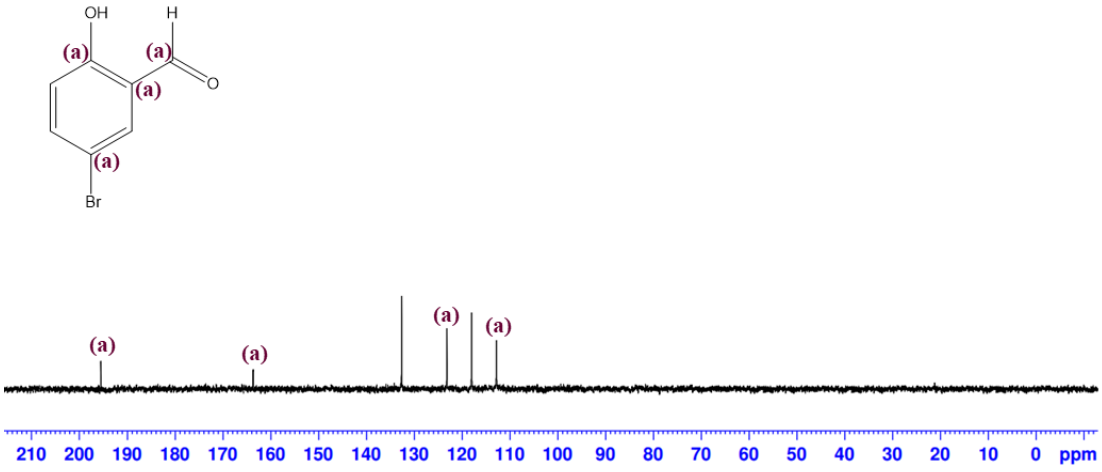

Fig. S21: [13]CNMR spectrum of 5-bromo-2-hydroxybenzaldehyde (Table-3, entry 10)

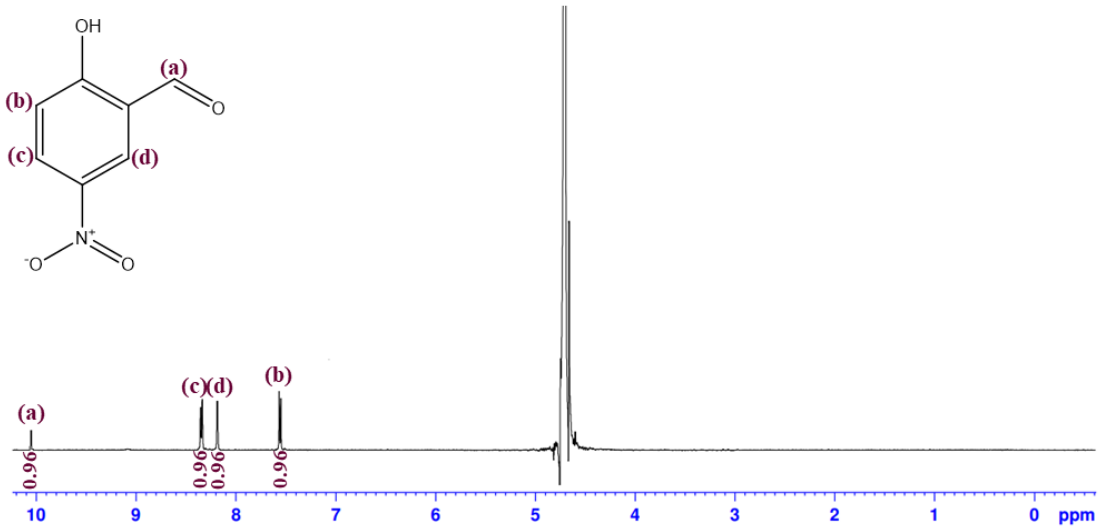

Fig. S22: ^{1}HNMR spectrum of 2-hydroxy-5-nitrobenzaldehyde (Table-3, entry 11)

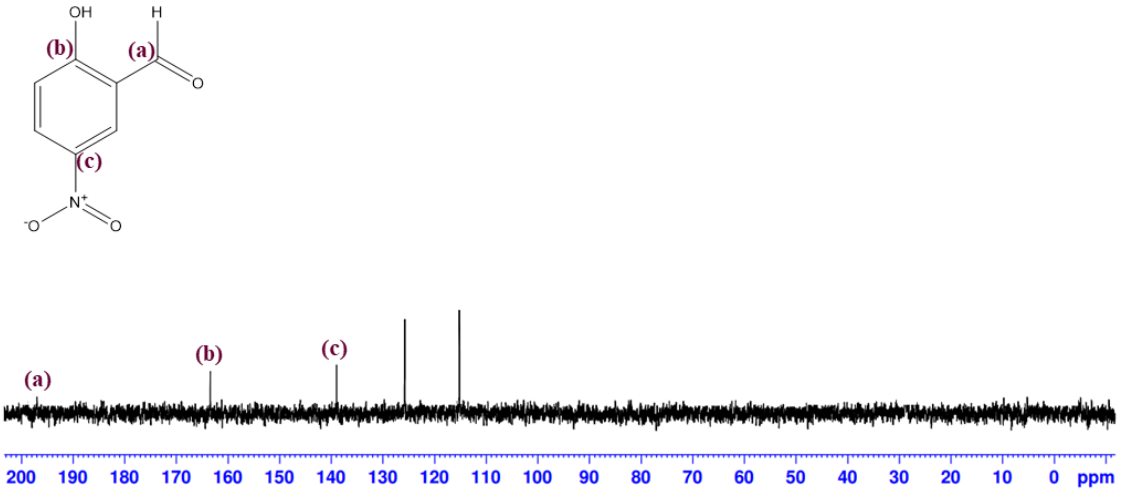

Fig. S23: ^{13}CNMR spectrum of 2-hydroxy-5-nitrobenzaldehyde (Table-3, entry 11)

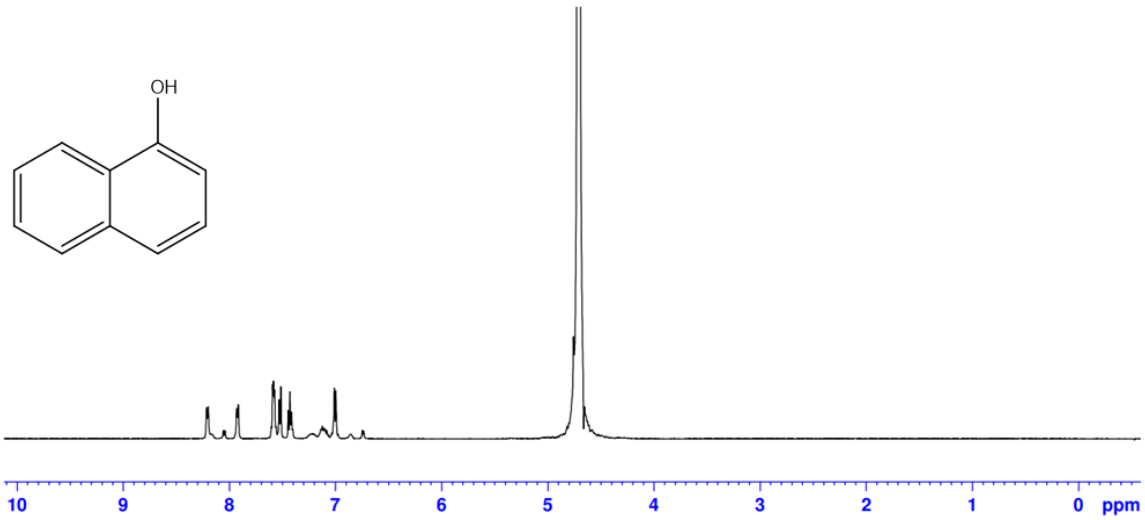

Fig. S24: [1]HNMR spectrum of 1-hydroxy-2-napthaldehyde (Table-3, entry 14)

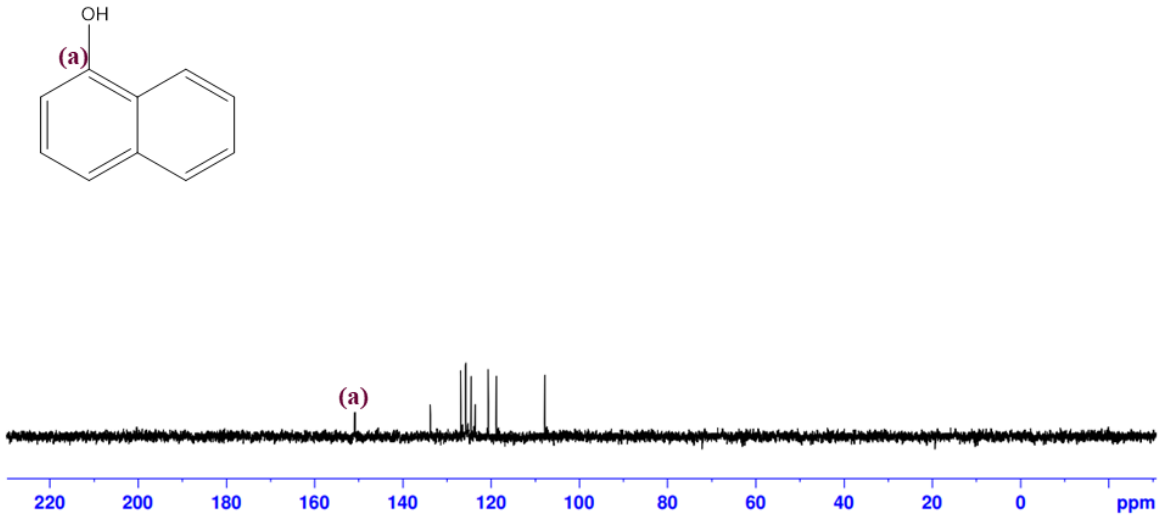

Fig. S25: [13]CNMR spectrum of 1-hydroxy-2-napthaldehyde (Table-3, entry 14)